Contents

Transport and mixing in the stratosphere: the role of Lagrangian studies

Bernard Legras and Francesco d'Ovidio

Laboratoire de Meteorologie Dynamique, Ecole Normale Supérieure and CNRS, 24 rue Lhomond, 75231 Paris Cedex 05, France legras@lmd.ens.fr, www.lmd.ens.fr/legras

1 Introduction

The stratosphere is an important component of the climate system which hosts 90% of the ozone protecting life from the ultra-violet radiations and, through the region called upper troposphere / lower stratosphere (UTLS) that encompasses the tropopause, has some control on the weather, the chemical composition of the atmosphere and the radiative budget. Because the temperature grows with altitude in the stratosphere, convection is inhibited by stratification, and the motion is mainly layerwise on isentropic surfaces, with time scales of the order of weeks to months. The cross-isentropic diabatic circulation is slow with time scales of the order of the season to several years. Below 30km, many chemical species, among which ozone, do not have significant sources or sinks and exhibit a chemical life-time of the order of several months to years. Such species can be treated as passive scalars transported by the flow. Their distribution is then dependent on the transport and mixing properties. Two useful quantities are the potential temperature $\theta = T(p_0/p)^{R/C_p}$ which is related to entropy by $S = C_p \ln \theta$ and the Ertel potential vorticity (or PV) $P = (\boldsymbol{\nabla}\times\mathbf{u}\cdot\boldsymbol{\nabla}\theta)/\rho$ which is a passive tracer under adiabatic and inviscid approximation. Owing to the separation between fast horizontal adiabatic motion and slow vertical diabatic motion, the potential temperature is often used as a vertical coordinate. PV is not practically measurable by in situ or remote instruments unlike many chemical tracers but can be easily calculated from model's output. It is most often used as a diagnostic of transport and dynamical activity.

Observations by in situ instruments and remote sensing show that the stratosphere exhibits well-mixed regions separated by transport or mixing barriers. Particularly, in the winter hemisphere, two dominating barriers are formed at the periphery of the polar vortex and in the subtropics that isolate the mid-latitudes from both the polar and tropical regions [1]. Since vertical, diabatically induced, motion is upward in the tropics and downward in the extra tropics, with the largest descent within the polar vortex, vertical tracer

gradients are turned into step horizontal gradients on isentropes intersecting the barriers. In the UTLS, the barrier associated with the subtropical jets near 30N and 30S in latitude separates the upper troposphere from the lowermost stratosphere on isentropic surfaces crossing the tropopause. The layer of the stratosphere just above the tropopause undergoes exchanges with the mid-latitude troposphere mainly due to upper level frontogenesis, which is a consequence of baroclinic instability and/or intense convective events which are often themselves associated with frontogenesis. At higher levels, that is for $380K > \theta > 350K$, the exchanges across the tropopause occur between the lower stratosphere and the Tropical Tropopause Layer (TTL) which is an intermediate region between the tropical convective layer and the stratosphere. Figure 1 summarizes these processes.

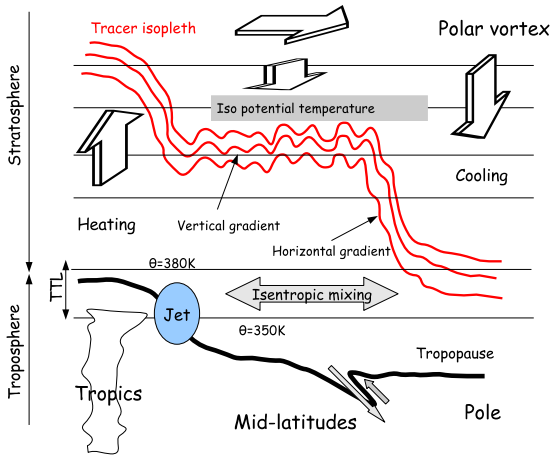

Fig. 1. Scheme summarizing the Brewer-Dobson meridional circulation in the stratosphere end exchange processes.

The scope of theory and modelling is to provide a qualitative and quantitative account of these observed properties. A number of progresses in this matter over the last ten years have been due to the extensive usage of Lagrangian calculations of parcel trajectories based on the analysed winds provided by the operational meteorological centers. It is the goal of this presentation to review the ongoing work in this direction.

2 Isentropic stirring

The strong stratification of the stratosphere accompanied by weak net diabatic contribution constrains parcels to move on isentropic surfaces. Lagrangian isentropic motion differs from fully turbulent motion and is akin

to two-dimensional turbulence or chaotic motion in a plane, where the flow is smooth and advection is dominated by the large structures. Such dynamics is known to produce transport barriers where tracer gradients intensify.

The effective diffusivity [2, 3, 4] has been used with success as a diagnostic of such effects in atmospheric flows. The method applies to a tracer, usually PV, with a mean latitudinal gradient such that the longitude-latitude coordinates can be replaced by the area of embedded tracer contours and an azimuthal coordinate along the contours. By a weighted averaging along the contours, the advection-diffusion equation $\partial c/\partial t + \mathbf{u}\boldsymbol{\nabla} c = \kappa \nabla^2 c$ is replaced by a purely diffusive equation

$$\frac{\partial C(A,t)}{\partial t} = \frac{\partial}{\partial A}\left(\kappa_{\rm eff}(A,t)\frac{\partial C(A,t)}{\partial A}\right),$$

where A is the area of the contour $\gamma(C,t)$ and the effective diffusivity is

$$\kappa_{{\rm eff}(A,t)} = \kappa_0 \frac{L^2_{\rm eq}(A,t)}{A\left(4\pi - \frac{A}{r^2}\right)} \tag{1}$$

with

$$L_{\rm eq}(A,t) = \oint_{\gamma(C,t)} |\nabla c| dl \oint_{\gamma(C,t)} \frac{1}{|\nabla c|} dl\,,$$

and r is the radius of the Earth. The device in (1) is to bind the complex stirring of the passive scalar in the averaging over the contour. It can be shown [5] that $L_{\rm eq}$ is always larger than the actual length of the tracer contour but that in practice the two quantities scale similarly. Hence, effective diffusivity is small where the contours are less deformed, that is where transverse gradients are less intensified, leading to less mixing.

Another measure of atmospheric stirring is provided by the local Lyapunov exponent [6, 7] which estimates the Lagrangian stretching as the separation rate of two close parcels over a given period of time or over a given growth. Around the Antarctic stratospheric polar vortex a minimum in both the effective diffusivity and local Lyapunov exponent is observed along the streak lines at the center of the jet [7, 8]. This minimum is surrounded by a very active mixing region with large stretching where air is brought from and to the mid-latitudes within a few days. However, the very stable Antarctic polar vortex is rather an exception than the rule among atmospheric flows which usually exhibit much less stable patterns. Over most of the atmosphere, the Lyapunov exponents and effective diffusivity are rather anti-correlated than correlated, contrary to the simple expectation.

The main reason of this discrepancy is that atmospheric flow, like most quasi-2D flows, is dominated by extended shear regions that stretch material lines but contribute weakly to the growth of tracer gradients. Let us first consider the deformation of a small material circle surrounding a parcel at time t. As time runs forward or backward, the flow defines a pair linear transformations T and T^{-1} which map the circle onto ellipses at future or past time

$t+\tau$ or $t-\tau$. The local forward and backward Lyapunov exponents are $\lambda_f = 1/\tau \ln \sigma_f$ and $\lambda_b = 1/\tau \ln \sigma_b$ where σ_f and σ_b are the singular values of T and T^{-1}. The singular vectors of these transformations are the Lyapunov eigenvectors. The eigenvector pointing to the smallest axis of the ellipse in the transformation indicates the unstable manifold or stable material line for backward time and the stable manifold or unstable material line for forward time [9, 8]. The convergence of the eigenvectors is at least as fast and generally much faster than the Lyapunov exponent [10]. Consquently, the tracer gradient tends, at any time, to be perpendicular to the local unstable manifold [11, 12]. This leads to an estimate of the future growth of the tracer gradient as the product of the forward Lyapunov exponent with the sine of the angle between the local stable and unstable manifolds that we denote as $\lambda_\perp$, the *transverse Lyapunov exponent*. Since stable and unstable manifolds are parallel in the direction of the wind for a pure shear, the transverse Lyapunov exponent vanishes in this case. As a matter of fact, when the gradient is perpendicular to the shear, it does not intensify at all.

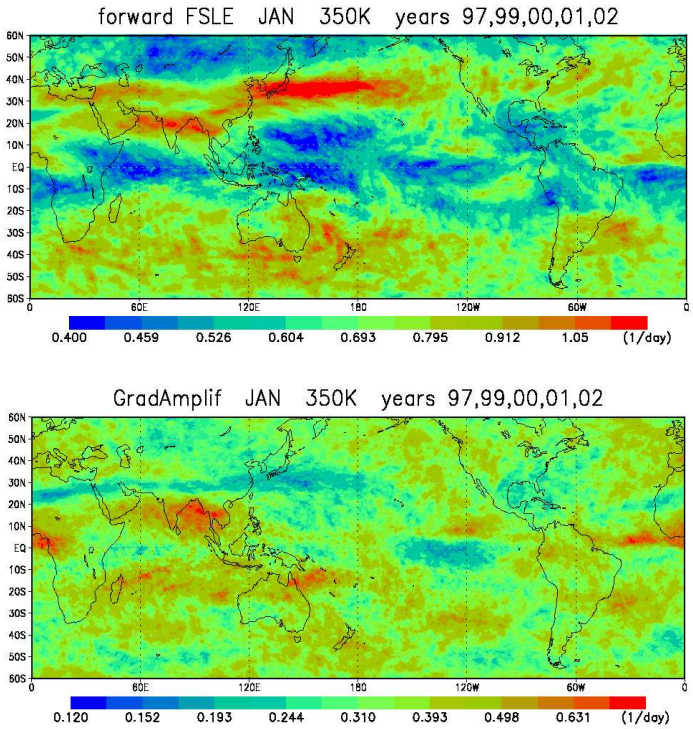

Fig. 2. Forward Lyapunov exponent (top), measuring stretching intensity, and transverse Lyapunov exponent (bottom) averaged over five January months on the surface $\theta = 350$K which intersects the tropopause within the subtropical jet.

Fig. 2 shows, strikingly, that that the maximum in stretching over the subtropical jet in the northern hemisphere (near 30N) is turned into a minimum of the transverse Lyapunov exponent, in agreement with the fact revealed from effective diffusivity that the jet acts as a barrier to mixing.

Fig. 3 shows that the transverse Lyapunov exponent correlates linearly with $\ln \kappa_{\rm eff}$ while no correlation emerges with the Lyapunov exponent.

A quantitative relation between effective diffusivity and the transverse Lyapunov exponent can be found by assuming that, owing to the chaotic stirring by the atmospheric flow, $L_{\rm eq} \sim \exp(\lambda_\perp T_\kappa)$ where T_k is a characteristic time after which diffusion becomes dominant and balances the exponential growth. Using this expression in (1), we define the *Lyapunov diffusion* κ_λ as

$$\ln \frac{\kappa_\lambda}{\kappa_0} = A + 2\lambda_\perp T_\kappa \tag{2}$$

where A is a constant. Both A and T_k can be obtained by a fit of κ_λ to $\kappa_{\rm eff}$. Fig.4 shows that indeed κ_λ reproduces very well the variations of $\kappa_{\rm eff}$.

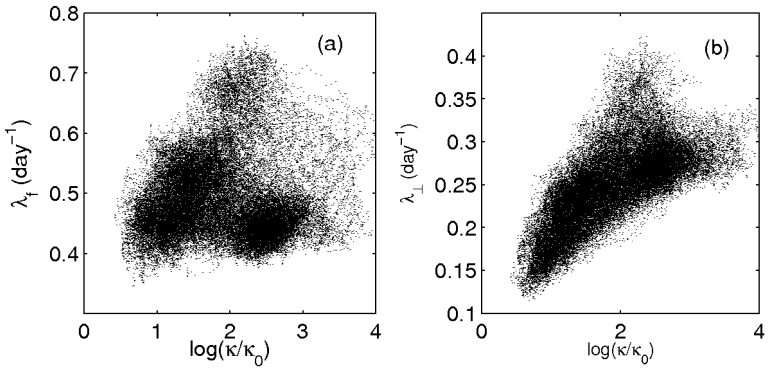

Fig. 3. Scatter plots of monthly-means of longitudinally averaged forward (a) and transverse (b) Lyapunov exponent against effective diffusivity over the period 1980-2000 on the θ =350K isentropic surface.

Hence transverse Lyapunov provides a diagnostic of atmospheric stirring that matches very well the effective diffusivity but with a number of advantages with respect to this latter, in particular in resolving structures in longitude. This is visible in Fig. 2 where the belt of low values along the jet is interrupted in the eastern Pacific opening a gate to mixing across this region between high and low latitudes. During the strong El Niño event of 1998, Fig. 5 shows a much more continuous belt over the Pacific, suggesting that El Niño is associated with a closing of the mixing gate. This result is also supported by analysis of meridional fluxes [13] and the climatology of intrusions of stratospheric air in the tropical upper troposphere [14]. For further discussion, see [15].

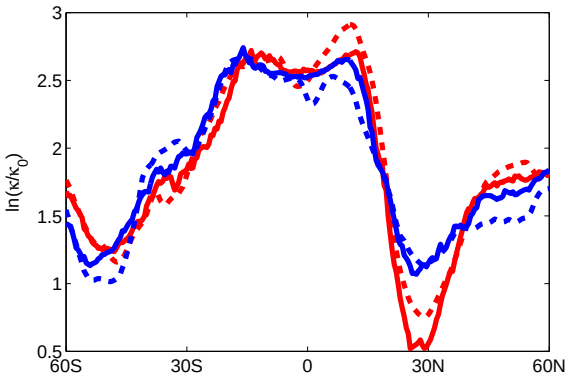

Fig. 4. Zonally averaged Lyapunov diffusivity (continuous line) and effective diffusivity (dashed line) for the El Niño winter 1997-1998 (red) and La Niña winter 1998-1999 (blue).

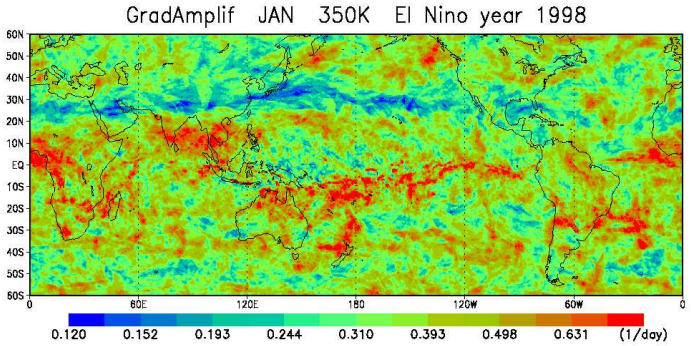

Fig. 5. Transverse Lyapunov exponent averaged over January 1998 on the surface θ =350K.

3 Vertical mixing

In the previous section, we diagnosed the stirring of tracers by layerwise motion that elongates tracer contours and generates a large number of filamentary structures within an isentropic surface. It has been shown [16, 17] that filaments are merely the horizontal section of sloping sheets with large horizontal to vertical aspect ratio of the order of 200. This value is essentially the ratio of the vertical shear to the horizontal strain. Owing to this high aspect ratio, the dissipation of a tracer sheet is mainly a product of vertical mixing by small-scale turbulence. Present meteorological analysis provided by weather centers basically resolve the motion that induces stirring and generation of tracer sheets, but small-scale turbulence due to shear instability or gravity wave breaking is unresolved by any large-scale numerical atmospheric model.

Local diffusion coefficient that may vary in space and time are often used to characterize the mixing produced by turbulence. Radar estimates of this quantity in active turbulent regions provide values of the order of 1-5 m^2s^{-1} but models [18, 17, 19] suggest that active regions are sparse in the atmosphere and that, on the average, much smaller turbulent diffusion is required to explain the observation of tracers.

Lagrangian reconstruction methods are often used to explain the spatial and temporal variations of atmospheric tracers. Such methods, sketched in Fig. 6, are based on the possibility to reconstruct small scales of the tracer distribution from the time series of the advecting wind and have been very successful in the lower stratosphere and the upper troposphere [20, 18, 21] showing that a large number of tracer structures seen in satellite images, aircraft transects and balloon profiles can be explained by advection. In most early studies, the reconstructed tracer was PV but recent works focuse on reconstructed chemical tracers that can be compared more directly with observations. Diffusion can be introduced in such methods by dividing each parcel into a large number of particles which are advected backward adding a random velocity component in the vertical direction, such that over one time step

$$\delta z = w\delta t + \eta\delta t\,,$$

where the random component η fits a chosen vertical turbulent diffusivity by [19]

$$D = \frac{1}{2} < \eta^2 > \delta t\,.$$

The rationale of this approach is to integrate the adjoint equation for the Green function of the advection-diffusion equation which is well-posed for backward times [19]. It has been applied, using a different formulation, to identify pollution sources from a network of sensors [22].

Comparing high resolution airborne tracer measurements with such reconstructions done with several values of D provides an estimate of the Lagrangian averaged diffusivity which matches best the observed fluctuations. Fig. 7 provides an example of such comparison done during a campaign in the Arctic, showing that turbulent diffusivity is, on the average, much smaller inside the polar vortex than outside, the largest of these estimates being one order of magnitude less than the radar estimate. When sharp transitions are identified in both the observed and the reconstructed data, it is possible to provide a local estimate of Lagrangian turbulent diffusivity. Fig .8 shows that D varies by at least one order of magnitude across a 80km wide filament.

As diffusivity can be estimated independently from the strain, a relation between both quantity, which is usually assumed in most parametrization of turbulence, can be tested. It has been shown [19] that on the average the two quantities are correlated but that this cannot explain the type of variability shown in fig. 8 which is perhaps due to burst of gravity wave breaking.

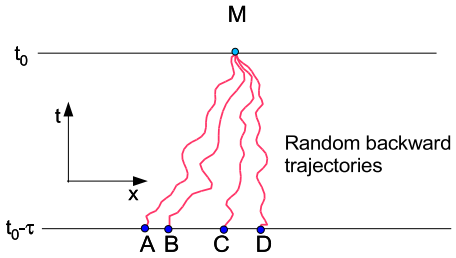

Fig. 6. In the standard reverse domain filling method [23] parcel trajectories starting at time t are integrated backward in time for a duration τ using available wind fields over the time interval. Provided a coarse resolution distribution of the tracer is known at time $t-\tau$, the value attributed to the parcel at time t is that of the coarse field at its location at time $t-\tau$. This procedure is able to reconstruct the small-scales at time t if transport is dominated by the resolved scales of motion. In the diffusive version [19], each parcel is a mixture of a cloud of particles that originate from a distribution of locations at time $t-\tau$ under backward advection plus diffusion. Then the value of the tracer at time t is an average of the values at $t-\tau$ for all the particles of the cloud. Unlike the standard procedure, the reconstruction is to a large extend independent of τ and the applied diffusion controls its smoothness.

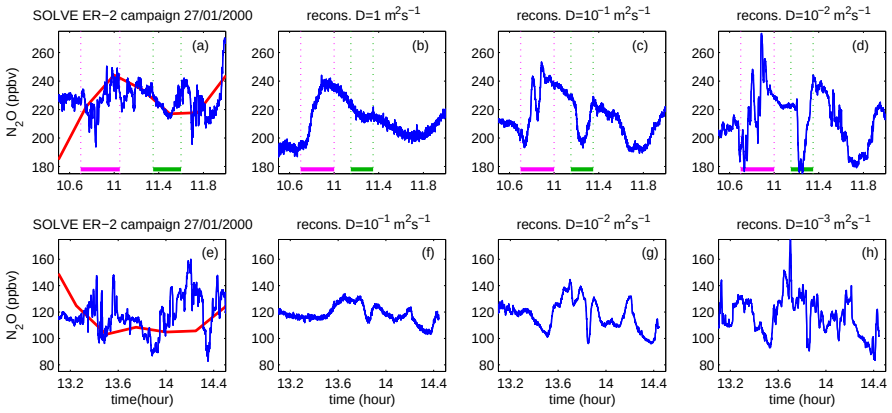

Fig. 7. (a): Sample of aircraft tracer measurement at 56 hPa in the surf zone outside the polar vortex during SOLVE campaign (winter 2000). In red the corresponding transect in the chemical transport model used to provide the coarse distribution of the tracer. (b-d): Advective-diffusive reconstructions for three values of the diffusivity $D = 1$, 0.1 and 0.01 $m^2\ s^{-1}$. The comparison is based on the roughness of the curves with some details identified near 11UT and 11:30UT. Clearly, the reconstruction is too smooth for $D = 1\ m^2\ s^{-1}$and too rough for $D = 0.1\ m^2\ s^{-1}$, while $D = 0.1\ m^2\ s^{-1}$seems of the right order. For a more quantitative assessment, see [19]. (e): Same as (a) inside the polar vortex. (f-h) Advective reconstructions inside the polar vortex where the comparison suggests that $0.01\ m^2\ s^{-1} > D > 0.001\ m^2\ s^{-1}$.

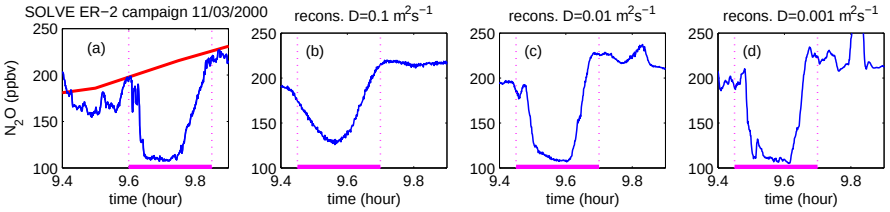

Fig. 8. (a) Tracer transect across a filament just outside the polar vortex during SOLVE campaign. The right edge of the filament fits very well an error function (solution of the advective diffusive equation with constant strain) with a width of 36km while the left edge is much steeper with a width of about 2.5km. (b-d) The reconstructions show that the two slopes cannot be reproduced with a single uniform diffusion indicating a large variation, by more than one order of magnitude, of turbulent diffusion across the width of the filament.

4 Meridional Brewer-Dobson circulation

Over time scales of several years the stratospheric circulation is characterized by an overturning from the tropics to the mid and polar latitudes (see Fig.1) known, since the pioneering work of Brewer [24], as the Brewer-Dobson circulation. It is an important requirement, for the distribution of long-lived chemical species that numerical models reproduce quantitatively this circulation. A large class of models of atmospheric chemistry, denoted as chemical-transport models, rely on the analysed winds provided by the operational weather centers to advect the chemical compounds horizontally and vertically. Among those wind datasets, the ERA-40 reanalysis of the European Center for Medium Range Weather Forecast (ECMWF), already used in section 1, is particularly useful since it covers a 45-year period from 1957 to 2002 [25].

Most global weather forecast models, including that of ECMWF, use the hydrostatic approximation. This means that vertical velocities are calculated from the the continuity equation, that is basically from the vertical integration of the horizontal divergence. Such estimate is known to be noisy by nature as the divergent circulation is weak and badly constrained by observations. Moreover, the practice of weather centers is to archive instantaneous velocity fields at times separated by interval of several hours, hence strongly undersampling fluctuations, such as gravity waves, with time scales much shorter than the archiving interval. Most studies indeed rely, by tradition, on 6-hourly winds. Fig .9 shows that these winds induce a too strong meridional circulation (hence the age is too young in the extra-tropics). However, a 3-hourly dataset, also available from ECMWF reduces considerably the discrepancy with observations. A chemical-transport model using this dataset is able to reproduce with good accuracy the ozone column at mid-latitude (F. Lefèvre, 2005, personal communication). Since the 3-hourly dataset still contains a significant amount of spurious noise, an alternative is to move horizontally parcel

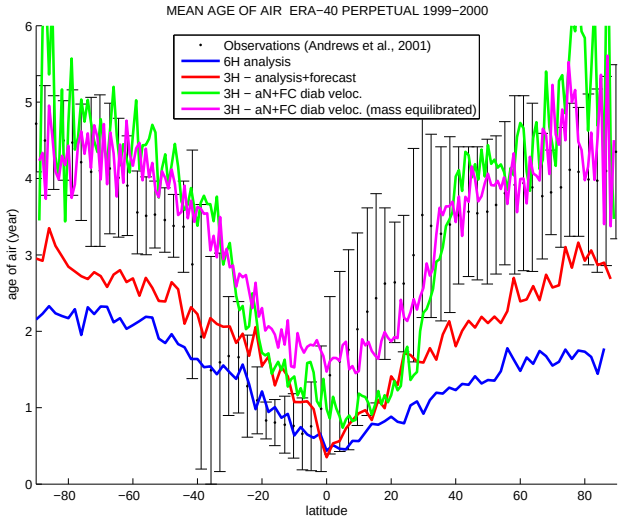

Fig. 9. Comparison of the age of air between observations and model calculations. The age of an air parcel is the time spent by this parcel in the stratosphere since it entered it at tropical latitudes [26]. Since an air parcel is a mixture, the mean age of air is the average over all particles within the parcel. The age of air can be measured using gases like SF_6, CH_4 and N_2O which are well mixed in the troposphere and are slowly destroyed in the stratosphere or CO_2 which is also well mixed in the troposphere and increases with time. The observation curve [27] is based an aircraft measurements at about 20km. Model calculations are performed using Lagrangian trajectories initialised almost uniformly at 20km integrated backward until they cross the tropopause. The age is averaged over latitude circles. The four curves are built using wind datasets over the cycle 1999-2000 and calculations are done over 15 years repeating this cycle. For parcels which have not left the stratosphere after 15 years, the age is extrapolated as in [28]. Blue: reconstruction using the ERA-40 winds at 6-hour interval. Red: reconstruction using the ERA-40 winds at 3-hour intervals (with forecasts interleaved with analysis as in [19]. Green: reconstruction using the ERA-40 winds in the horizontal and heating rates for vertical motion. Magenta: same as previous with a correction on the horizontal isentropic divergence to balance the hearting rate.

on isentropic surfaces and to use diabatic heating rates, calculated from the local radiative budget and averaged over 3-hour intervals, as vertical velocities. Fig 9 shows that the meridional circulation calculated from such data provides a good agreement with observations. Doing so, we have, however, introduced an inconsistency since mass conservation is no longer satisfied. This conservation is reestablished by forcing the horizontal divergence on isentropic surfaces to satisfy the equation

$$\partial\sigma/\partial t + \boldsymbol{\nabla}_\theta(\sigma\mathbf{u}) + \partial(\sigma\dot{\theta})/\partial\theta = 0$$

where $\sigma = -g\partial p/\partial\theta$. Fig. 9 shows that a further improvement in the agreement with observations is obtained in this way except near the equator. Hence, it is now clear that available analyses fulfill the constrain that the Brewer-Dobson circulation is fairly well reproduced, at least over the recent years where high quality satellite observations are available, but it is also clear that special care should be taken when using analysed data for transport calculations over durations of months to years in order to avoid spurious diffusive transport due to noise and undersampling. Another important factor impacting the quality of the analysis is the the model itself and the type of assimilation scheme [28, 29].

References

[1] L. Polvani, D. Waugh, R. Plumb, On the subtropical edge of the stratospheric surf zone, J. Atmos. Sci. 51 (11) (1995) 1401–1416.

[2] N. Nakamura, Two-dimensional mixing, edge formation, and permeability diagnosed in an area coordinate, J. Atmos. Sci. 53 (11) (1996) 1524.

[3] P. Haynes, E. Shuckburgh, Effective diffusivity as a diagnostic of atmospheric transport. Part I: stratosphere, J. Geophys. Res. 105 (D18) (2000) 22,777–22,794.

[4] P. Haynes, E. Shuckburgh, Effective diffusivity as a diagnostic of atmospheric transport. Part II: troposphere and lower stratosphere, J. Geophys. Res. 105 (D18) (2000) 22,795–22,810.

[5] E. Shuckburgh, P. H. Haynes, Diagnosing transport and mixing using a tracer-based coordinate system, Phys. Fluids 15 (2003) 3342–3357.

[6] R. Pierrehumbert, Large-scale horizontal mixing in planetary atmospheres, Phys. Fluids A 3 (5) (1991) 1250–1260.

[7] B. Joseph, B. Legras, Relation between kinematic boundaries, stirring, and barriers for the Antarctic polar vortex, J. Atmos. Sci. 59 (2002) 1198–1212.

[8] T.-Y. Koh, B. Legras, Hyperbolic lines and the stratospheric polar vortex, Chaos 12 (2) (2002) 382–394.

[9] G. Haller, G. Yuan, Lagrangian coherent structures and mixing in two-dimensional turbulence, Physica D 147 (2000) 352–370.

[10] B. Legras, R. Vautard, A guide to Liapunov vectors, in: Predictability, Vol. I of Seminar Proceedings, ECMWF, Reading, UK, 1996, pp. 143.

[11] P. Klein, B. L. Hua, G. Lapeyre, Alignment of tracer gradient vectors in 2d turbulence, Physica D 146 (2000) 246–260.

[12] G. Lapeyre, B. Hua, P. Klein, Dynamics of the orientation of active and passive scalars in two-dimensional turbulence, Ph. Fl. 13 (2001) 251–264.

[13] M. Shapiro, H. Wernli, N. Bond, R. Langland, The influence of the 1997-1998 ENSO on extratropical baroclinic life cycles over the Eastern North Pacific, Quart. J. Roy. Met. Soc. 127 (2001) 331–342.

[14] D. Waugh, L. Polvani, Climatology of intrusions into the tropical upper troposphere, Geophys. Res. Lett. 27 (23) (2000) 3857–3860.

[15] F. d'Ovidio, B. Legras, E. Shuckburgh, Local diagnostic of mixing and barrier modulation at the tropopause, submitted to Geophys. Res. Lett., http://www.lmd.ens.fr/legras (2006).
[16] D. Waugh, R. Plumb, R. Atkinson, M. Schoeberl, L. Lait, P. Newman, M. Lowenstein, D. Toohey, L. Avallone, C. Webster, R. May, Transport of material out of the stratospheric Arctic vortex by Rossby wave breaking, J. Geophys. Res. 99 (D1) (1994) 1071–1088.
[17] M. Balluch, P. Haynes, Quantification of lower stratospheric mixing processes using aircraft data, J. Geophys. Res. 102 (D19) (1997) 23,487–23,504, (97JD00607).
[18] D. Waugh, R. Plumb, J. Elkins, D. Fahey, K. Boering, G. Dutton, C. Volk, E. Keim, R.-S. Gao, B. Daube, S. Wofsy, M. Lowenstein, J. Podolske, K. Chan, M. Proffitt, K. Kelly, P. Newman, L. Lait, Mixing of polar air into middle latitudes as revealed by tracer-tracer scatter plots, J. Geophys. Res. 102 (D11) (1997) 13,119–13,134, (96JD03715).
[19] B. Legras, I. Pisso, G. Berthet, F. Lefèvre, Variability of the Lagrangian turbulent diffusion in the lower stratosphere, Atmos. Chem. Phys. 5 (2005) 1–18.
[20] C. Appenzeller, H. Davies, W. Norton, Fragmentation of stratospheric intrusions, J. Geophys. Res. 101 (D1) (1996) 1453–1456.
[21] A. Mariotti, M. Moustaoui, B. Legras, H. Teitelbaum, Comparison between vertical ozone soundings and reconstructed potential vorticity maps by contour advection with surgery, J. Geophys. Res. 102 (D5) (1997) 6131–6142.
[22] J. Issartel, J. Baverel, Inverse transport for the verification of the Comprehensive Nuclea Test Ban Treaty, Atmos. Chem. Phys. 3 (2003) 475–486.
[23] R. Sutton, H. Maclean, R. Swinbank, A. O'Neill, F. Taylor, High-resolution stratospheric tracer fields estimated from satellite observations using Lagrangian trajectory calculations, J. Atmos. Sci. 51 (1994) 2995.
[24] A. Brewer, Evidence for a world circulation provided by the measurements of helium and water vapour distribution in the stratopshere, Quart. J. Roy. Met. Soc. 75 (1949) 351–363.
[25] S. Uppala, *et al.*, The ERA-40 re-analysis, Quart. J. Roy. Met. Soc. 131 (2005) 2961–3012.
[26] D. Waugh, T. Hall, Age of stratospheric air: theory, observations, and models, Rev. Geophys. 40 (4).
[27] A. Andrews, *et al.*, Mean ages of stratospheric air derived from in situ observations of CO_2, CH_4, and N_2O, J. Geophys. Res. 106 (D23) (2001) 32,295–32,314.
[28] M. Scheele, P. Siegmund, P. van Velthoven, Stratospheric age of air computed with trajectories based on various 3D-Var and 4D-Var data sets, Atmos. Chem. Phys. 5 (2005) 1–7.
[29] B. Monge-Sanz, M. Chipperfiels, A. Simmons, S. Uppala, Mean age of air and transport in a CTM: comparison of different ECMWF analyses, submitted to Geophys. Res. Lett. (2006).